

## Control of 3 DOF Quadrotor Model

Tae Soo Kim, Karl Stol, and Vojislav Kecman

Department of Mechanical Engineering, The University of Auckland,  
Auckland, New Zealand

tkim020@ec.auckland.ac.nz, {k.stol,v.kecman}@auckland.ac.nz

### 2.1 Introduction

Unmanned aerial vehicles (UAVs) comprise various types of aircrafts such as conventional fixed-wing aircraft, helicopters, blimps, and airships. Among these, helicopters are classified as planar vertical take off and landing (PVTOL) aircraft by which it means that unlike a fixed-wing aircraft, it can take off and land in a limited space, hover in the air, and move sideways and backwards. This superior maneuverability allows performing important roles in many areas, which conventional aircraft could not achieve. The type of their useful work includes: dangerous applications such as in a war, victim rescue and volcano monitoring, where other types of vehicle are inaccessible, commercial application such as film making, and agricultural applications, farm monitoring and spreading chemicals [1]. The demand for UAVs keeps increasing. Unfortunately these exclusive maneuverability advantages give a big complexity and instability in its dynamics, hence making it hard to control. The development of a UAV is challenging, and it is an emerging area in nonlinear control study among researchers.

A few researchers focussed on applying various control techniques to a quadrotor. Lozano *et al.* [2] approached global stabilization of a PVTOL vehicle using Lyapunov analysis, designing a simple nonlinear controller by analysing boundedness and convergence of each state. Bouabdallah *et al.* [3, 4] built a micro VTOL autonomous robot, 'OS4'. OS4 was a three DOF model controlling only rotations. The Lyapunov theorem was used for controller design. Later they explored the application of two different techniques, PID and linear quadratic (LQ), to OS4. OS4 at near-hover condition was tested, neglecting gyroscopic effects from the rigid body and propeller rotation, i.e. removing all cross

couplings. Yang *et al.* [5] studied motion control of a quadrotor using time-optimal control (TOM). With TOM, the problem was to find inputs that would move the system from its initial configuration to a desired final configuration in minimum time.

Design and choice of sensors are an important aspect in UAV design. Pounds *et al.* [8] worked with blade designs to optimize the thrust generation and dynamic stability. Airfoil design and material properties of blades were studied and the flapping behaviour of a blade were analysed by adapting an existing mathematical model. Altug *et al.* [6, 7] studied motion control of a quadrotor through visual feedback using a camera.

At the University of Auckland, a number of undergraduate projects have been undertaken to study control of helicopter models. In 2003, R. Murphy and T. Hay [9] designed and controlled a rig that replicated pitching motion of a helicopter using a PID controller. In 2004 W. Zhao and T. Kim [11] worked on single DOF altitude control of a helicopter. Also in the same year, A. Stojanovic [10] constructed a 2-DOF helicopter model controlling pitch and yaw using a PLC (programmable logic controller). In 2006, D. Campbell and L. D'Souza [12] attempted to create a free-flying semi-autonomous quadrotor helicopter. With a micro controller programmed with a PD controller, the quadrotor was able to hover in the air for a few seconds, yet it was not stable enough for a free flight. Limitations of classical control on a complex dynamic plant were observed. In this research we aimed to develop control algorithms to stabilize an unstable quadrotor plant and implement this on an experimental rig. Four different control techniques are simulated and their performances are evaluated.

## 2.2 Modelling of Quadrotor

The Quadrotor in Fig. 2.1 can be modeled as a 6-DOF rigid body, with three translations, movement along X, Y, and Z coordinates, and three rotations, pitch, roll, and yaw, which are rotations about X, Y, and Z axes, respectively. The quadrotor is an underactuated system; there are fewer individual inputs than the DOF to be controlled. Some states are controlled through other states. The movement along the Y axis is controlled by the pitch angle  $\phi$ . Increasing the force  $F_4$  relative to  $F_2$ , while the sum of all four thrust balances the weight  $mg$  results in rotation in  $\phi$ , induces the movement of the body along the Y axis, the axis in body fixed frame  $B$  in Fig. 2.1. In a similar way, the movement along the X axis is controlled by the roll angle  $\theta$ . Movement along the vertical Z axis occurs by increasing the thrusts from all the four

rotors so that the collective thrust exceeds the weight of the rig. While doing this, the thrust from each rotor must balance the thrust from the opposite rotor. Rotors 1 & 3 rotate clockwise and rotors 2 & 4 rotate counter-clockwise to counter-balance the gyroscopic moments causing the rigid body rotation about the Z axis.

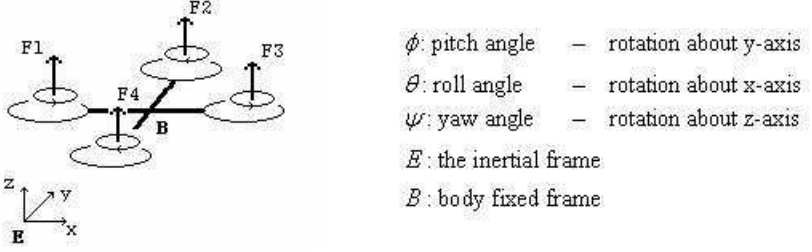


**Fig. 2.1.** Quadrotor configuration

Prior to simulation, a mathematical model for the quadrotor is derived. For the derivation, the notation from [3] is followed. The rotational dynamics of the quadrotor is expressed as:

$$\ddot{\phi} = \dot{\theta} \dot{\psi} \left( \frac{I_y - I_z}{I_x} \right) - \frac{J_p}{I_x} \dot{\theta} (\Omega_2 + \Omega_4 - \Omega_1 - \Omega_3) + \frac{l}{I_x} b (\Omega_4^2 - \Omega_2^2), \quad (2.1)$$

$$\ddot{\theta} = \dot{\phi} \dot{\psi} \left( \frac{I_z - I_x}{I_y} \right) + \frac{J_p}{I_y} \dot{\phi} (\Omega_2 + \Omega_4 - \Omega_1 - \Omega_3) + \frac{l}{I_y} b (\Omega_3^2 - \Omega_1^2), \quad (2.2)$$

$$\ddot{\psi} = \dot{\theta} \dot{\phi} \left( \frac{I_x - I_y}{I_z} \right) + \frac{l}{I_z} d (\Omega_2^2 + \Omega_4^2 - \Omega_1^2 - \Omega_3^2), \quad (2.3)$$

where  $I_x, y, z$  are the rotational inertias of the body,  $J_p$  is the rotational inertia of the propeller,  $\Omega$  is the angular speed of the rotor,  $l$  is the rotor position from the centre,  $b$  and  $d$  are thrust and drag coefficients, respectively.

The assumptions for this model are:

- the body is rigid and symmetrical;
- the centre of mass and the body fixed frame origin coincide;
- the propellers are rigid, i.e. no blade flapping occurs.

As the equations show there is coupling present between the rotational speeds of the body.

## 2.3 Experimental Setup

An experimental rig, as shown in Fig. 2.2, replicating the attitude of the quadrotor is designed to apply control algorithm. The design specification for the rig is:

- A 3-DOF model must fully replicate the rotational motion of the quadrotor. The translational DOFs are removed.
- The centre of mass of the rig must coincide with the centres of the three rotations. This is to ensure the resulting motions are pure rotations.
- The operating range for pitch and roll are  $\pm 40^\circ$  and  $\pm 180^\circ$  for the yaw.

Three optical incremental encoders, HP HEDS5700, are chosen for measuring individual rotations. A dSpace control board DS1104 is used for data acquisition and produces PWM control signals for the motors along with Simulink and Control Desk. The DS1104 supports two incremental encoder inputs and four PWM pulse generation. The extra encoder is interfaced through a digital bit I/O port. The motors, gears, propellers, and carbon fibre arms come from a commercial quadrotor design, the Dranganflyer V [13].

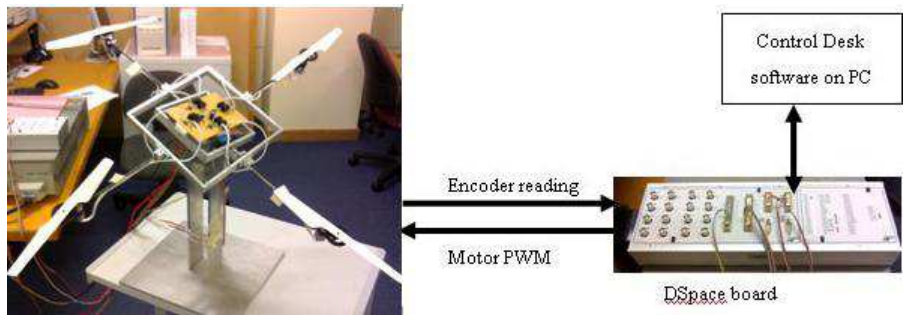


Fig. 2.2. Quadrotor experimental rig

## 2.4 Control Design

### 2.4.1 Optimal Control (LQR)

Linearization of the nonlinear quadrotor plant is the first step for deriving a linear control law. The plant is linearized about an equilibrium

point at which the three orientation angles  $\phi, \theta, \psi$  and its velocities  $\dot{\phi}, \dot{\theta}, \dot{\psi}$  are zero and the angular speeds of the four rotors are equal. The linearization results in:

$$\begin{bmatrix} \Delta \dot{\phi} \\ \Delta \dot{\theta} \\ \Delta \dot{\psi} \\ \Delta \ddot{\phi} \\ \Delta \ddot{\theta} \\ \Delta \ddot{\psi} \end{bmatrix} = \begin{bmatrix} 0 & 0 & 0 & 1 & 0 & 0 \\ 0 & 0 & 0 & 0 & 0 & 1 \\ 0 & 0 & 0 & 0 & 0 & 1 \\ 0 & 0 & 0 & 0 & 0 & 0 \\ 0 & 0 & 0 & 0 & 0 & 0 \\ 0 & 0 & 0 & 0 & 0 & 0 \end{bmatrix} \begin{bmatrix} \Delta \phi \\ \Delta \theta \\ \Delta \psi \\ \Delta \dot{\phi} \\ \Delta \dot{\theta} \\ \Delta \dot{\psi} \end{bmatrix} + \begin{bmatrix} 0 & 0 & 0 & 0 \\ 0 & 0 & 0 & 0 \\ 0 & 0 & 0 & 0 \\ 0 & -2b\frac{l}{I_x}\Omega_{ss} & 0 & 2b\frac{l}{I_x}\Omega_{ss} \\ -2b\frac{l}{I_y}\Omega_{ss} & 0 & 2b\frac{l}{I_y}\Omega_{ss} & 0 \\ -2d\frac{l}{I_z}\Omega_{ss} & 2d\frac{l}{I_z}\Omega_{ss} & -2d\frac{l}{I_z}\Omega_{ss} & 2d\frac{l}{I_z}\Omega_{ss} \end{bmatrix} \begin{bmatrix} \Delta \Omega_1 \\ \Delta \Omega_2 \\ \Delta \Omega_3 \\ \Delta \Omega_4 \end{bmatrix}. \quad (2.4)$$

The subscript  $ss$  denotes 'steady state'.

## 2.4.2 LQR with Gain Scheduling

Small sphere approximating approach for linearization is implemented with gain scheduling. Linearization is performed continuously to re-linearize about every operating point along the state trajectory [14]. The resulting matrix form is the same as above having the corresponding matrices as given below:

$$\mathbf{A} = \begin{bmatrix} 0 & 0 & 0 & 1 & 0 & 0 \\ 0 & 0 & 0 & 0 & 1 & 0 \\ 0 & 0 & 0 & 0 & 0 & 1 \\ 0 & 0 & 0 & 0 & I_1 \dot{\psi} - I_4 \bar{\Omega} & I_1 \dot{\theta} \\ 0 & 0 & 0 & I_2 \dot{\psi} + I_5 \bar{\Omega} & 0 & I_2 \dot{\phi} \\ 0 & 0 & 0 & I_3 \dot{\theta} & I_3 \dot{\phi} & 0 \end{bmatrix}, \text{ and } \mathbf{B} = \quad (2.5)$$

$$\begin{bmatrix} 0 & 0 & 0 & 0 \\ 0 & 0 & 0 & 0 \\ 0 & 0 & 0 & 0 \\ I_4 \dot{\bar{\theta}} & -(I_4 \dot{\bar{\theta}} + 2bI_6 \bar{\Omega}_2) & I_4 \dot{\bar{\theta}} & -I_4 \dot{\bar{\theta}} + 2bI_6 \bar{\Omega}_4 \\ -(I_5 \dot{\bar{\phi}} + 2bI_7 \bar{\Omega}_1) & I_5 \dot{\bar{\phi}} & -I_5 \dot{\bar{\phi}} + 2bI_7 \bar{\Omega}_3 & I_5 \dot{\bar{\phi}} \\ -2dI_8 \bar{\Omega}_1 & 2dI_8 \bar{\Omega}_2 & 2dI_8 \bar{\Omega}_3 & -2dI_8 \bar{\Omega}_4 \end{bmatrix}, \quad (2.6)$$

where  $I_1 = (I_y - I_z)/I_x$ ,  $I_2 = (I_z - I_x)/I_y$ ,  $I_3 = (I_x - I_y)/I_z$ ,  $I_4 = J_p/I_x$ ,  $I_5 = J_p/I_y$ ,  $I_6 = l/I_x$ ,  $I_7 = l/I_y$ ,  $I_8 = l/I_z$ . The bar above a symbol denotes its current value. This is more accurate linearization of the plant, but recalculating the state matrix, input matrix, and control gain  $K$  for every step is computationally expensive. The control law becomes  $\underline{u} = -K(t)\underline{x}$ , where  $K(t)$  is the time-varying control gain matrix.

### 2.4.3 Feedback Linearization

Using feedback linearization, nonlinear terms are cancelled out by the control input. The derived control inputs are:

$$U_1 = \frac{I_x}{l}(-\dot{\bar{\theta}}\dot{\bar{\psi}}\left(\frac{I_y - I_z}{I_x}\right) + \frac{J_p}{I_x}\dot{\bar{\theta}}(\Omega_2 + \Omega_4 - \Omega_1 - \Omega_3) - k_1x), \quad (2.7)$$

$$U_2 = \frac{I_y}{l}(-\dot{\bar{\phi}}\dot{\bar{\psi}}\left(\frac{I_z - I_x}{I_y}\right) - \frac{J_p}{I_y}\dot{\bar{\phi}}(\Omega_2 + \Omega_4 - \Omega_1 - \Omega_3) - k_2x), \quad (2.8)$$

$$U_3 = \frac{I_z}{l}(-\dot{\bar{\theta}}\dot{\bar{\phi}}\left(\frac{I_x - I_y}{I_z}\right) - k_3x), \quad (2.9)$$

where

$$U_1 = F_4 - F_2, \quad U_2 = F_3 - F_1, \quad U_3 = \frac{d}{b}(F_2 + F_4 - F_1 - F_3). \quad (2.10)$$

$F_1$  to  $F_4$  are the thrust forces from the four rotors as shown in Fig. 2.1. Equation (2.10) can be resolved into the individual forces using pseudo inversion.

### 2.4.4 Sliding Mode Control

The following sliding mode controller is developed to drive all the states to zero. The terms in the first bracket of Eqs. (2.11) through (2.13) cancel out the nonlinearities, while the following term with sign switches control input to keep the system in a stable manifold [15].

$$U_1 = -\frac{I_x}{l} \left( \dot{\theta} \dot{\psi} \frac{I_y - I_z}{I_x} - \frac{J_p}{I_x} \dot{\theta} (\Omega_2 + \Omega_4 - \Omega_1 - \Omega_3) + \alpha_1 \dot{\phi} \right) - K_1 \text{sign}(\dot{\phi} + \alpha_1 \phi), \quad (2.11)$$

$$U_2 = -\frac{I_y}{l} \left( \dot{\phi} \dot{\psi} \frac{I_z - I_x}{I_y} + \frac{J_p}{I_y} \dot{\phi} (\Omega_2 + \Omega_4 - \Omega_1 - \Omega_3) + \alpha_2 \dot{\theta} \right) - K_2 \text{sign}(\dot{\theta} + \alpha_2 \theta), \quad (2.12)$$

$$U_3 = -\frac{I_z}{l} \left( \dot{\theta} \dot{\phi} \frac{I_x - I_y}{I_z} + \alpha_3 \dot{\psi} \right) - K_3 \text{sign}(\dot{\psi} + \alpha_3 \psi). \quad (2.13)$$

Two control parameters  $\alpha$  and  $K$  in sliding mode control are tuned by simulating a range of parameter combinations for the minimum ITSE (Integral of Time multiplied by Square of Error).

## 2.5 Simulations

Simulations were run in Simulink for all the four previously derived controllers. The controllers are set to regulate all states. The initial conditions are:  $\phi = 0.5$ ,  $\theta = 0.3$  rad,  $\psi = -0.2$  rad. The control parameters for each controller are tuned to return the least possible ITSE index in state regulation. For numerical comparisons the performance index ITSE is used with total control effort. Each controller is tuned to return the least possible ITSE index. Figure 2.3 shows the simulation result for the four types of controllers in state regulation in pitch orientation. Figure 2.4 shows the responses with uncertainty introduced to plant parameters.

Tables 2.1 and 2.2 summarize the performance of the four different control techniques. With accurate plant parameters, sliding mode controller returns the best result. It is evident that a better response is obtained with larger control effort but relatively small percentage changes in total control effort indicate that the effort required to improve orientation control is much smaller than that for balancing the gravitational force. On the other hand, with model uncertainty introduced, the performance of sliding mode controller deteriorates and the performance of LQR with gain scheduling becomes outstanding.

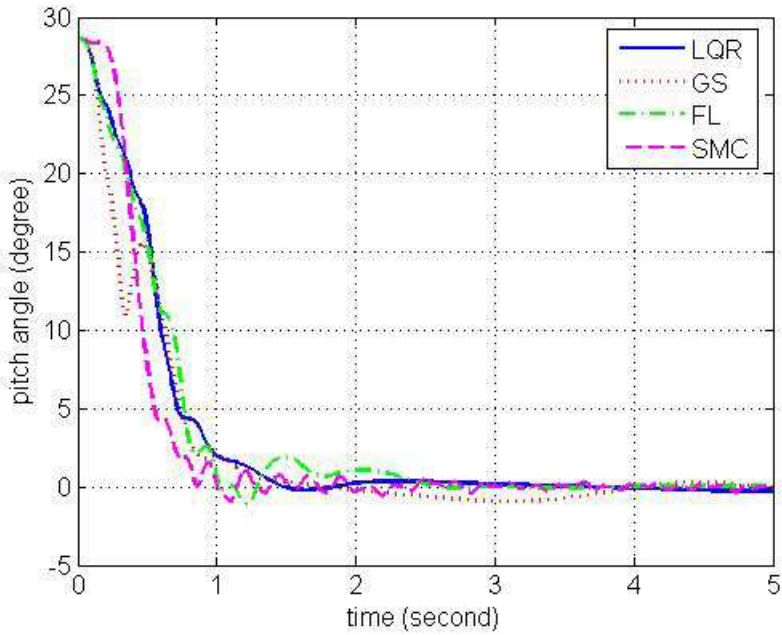


Fig. 2.3. Simulation result for four controllers in state regulation

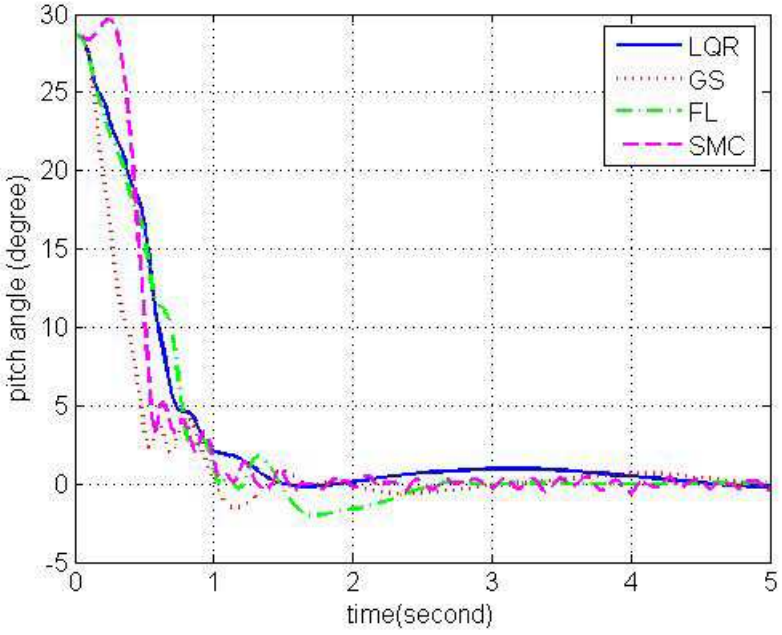


Fig. 2.4. Simulation result for controllers with model uncertainty

**Table 2.1.** ITSE values and total control efforts in state regulation

Controller	ITSE index	% difference	$\Sigma u(t) $	% difference
LQR	0.3018	0	479.3	0
Gain Schedule	0.2491	-17.5	482.7	+0.7
Feedback Lin.	0.3291	+9.1	472.9	-1.3
Sliding Mode	0.2186	-27.6	495.7	+3.4

**Table 2.2.** ITSE values and total control efforts with model uncertainty

Controller	ITSE index	% difference	$\Sigma u(t) $	% difference
LQR	0.3180	0	479.7	0
Gain Schedule	0.2320	-27.0	481.8	+0.4
Feedback Lin.	0.3488	+9.7	473.0	-1.4
Sliding Mode	0.3078	-3.2	496.3	+3.5

## 2.6 Conclusions

In this paper, four different control techniques: LQR, LQR with gain scheduling, feedback linearization, and sliding mode control were derived and simulated on a 3-DOF quadrotor model. Compared under ITSE criteria, sliding mode control produced the best result with accurate plant model, while LQR with gain scheduling showed robustness against the model uncertainty. It is concluded that nonlinear control techniques have greater dependency on accurate model estimation. The quadrotor model is currently undergoing a gain tuning stage. The simulation results will be tested on the experimental rig for real-time result and further comparison is to be done. Our experimental rig can be further improved in the future by reducing the weight and using other sensor combination for a complete 6-DOF free-flying quadrotor.

## References

1. Sugiura R, Fukagawa T, Noguchi, N (2003) Field Information System Using an Agricultural Helicopter towards Precision Farming. Proc IEEE/ASME Int. Conf. on Advanced Intelligent Mechatronics 1073–1078
2. Lozano R, Castillo P, Dzul A (2004) Global stabilization of the PVTOL: real-time application to a mini-aircraft. Int. Journal of Control 77-8: 735–740
3. Bouabdallah S, Noth A, Siegwart R (2004) PID vs LQ Control Techniques Applied to an Indoor Micro Quadrotor. Proc. IEEE Int. Conf. on Intelligent Robots and Systems

3. Bouabdallah S, Noth A, Siegwart R (2004) PID vs LQ Control Techniques Applied to an Indoor Micro Quadrotor. Proc. IEEE Int. Conf. on Intelligent Robots and Systems
4. Bouabdallah S, Murrieri P, Siegwart R (2004) Design and Control of an Indoor Micro Quadrotor. Proc. Int. Conf. on Robotics and Automation.
5. Yang C, Lai L, Wu C (2006) Time-Optimal Control of a Hovering Quadrotor Helicopter. *Journal of Intelligent and Robotic Systems* 45: 115–135
6. Altug E, Ostrowski J, Mahony R (2002) Control of a Quadrotor Helicopter Using Visual Feedback. Proc. Int. Conf. on Robotics & Automation.
7. Altug E, Ostrowski J, Taylor C (2003) Quadrotor Control Using Dual Camera Visual Feedback. Proc. Int. Conf. on Robotics & Automation.
8. Pounds P, Mahony R, Gresham J (2004) Towards Dynamically-Favourable Quad-Rotor Aerial Robots. Proc. Australian Conf. Robotics and Automation.
9. Murphy R, Hay T (2003) Helicopter Pitch Control. Final year project report, The University of Auckland.
10. Stojanovic A (2004) Two Degrees of Freedom Helicopter Controlled by a Programmable Logic Controller. ME Thesis, The University of Auckland.
11. Kim T, Zhao V (2004) Helicopter Height Control. Final year project report, The University of Auckland.
12. Campbell D, D'Souza L (2006) Design and Control of a Miniature Four Rotor Helicopter. Final year project report, The University of Auckland.
13. Draganfly Inovations Inc. supplier. url: <http://www.rctoys.com/>
14. Zheng J (2006) Comparison of Two Linearization Methods for Optimal attitude manoeuvre of a non-linear flexible spacecraft. *IMA Journal of Mathematical Control and Information* 127–136
15. Khalil HK (2002) *Nonlinear Systems*. third edition, Prentice Hall